Journal of Marine Science and Technology

Volume 26 | Issue 4 Article 7

SENSITIVITY ANALYSIS OF STEEP WAVE RISER WITH INTERNAL FLOW

Zhen Liu
College of Engineering, Ocean University of China, Qingdao, China

Haiyan Guo
College of Engineering, Ocean University of China, Qingdao, China, hyguo@ouc.edu.cn

Recommended Citation

Liu, Zhen and Guo, Haiyan (2018) "SENSITIVITY ANALYSIS OF STEEP WAVE RISER WITH INTERNAL FLOW," *Journal of Marine Science and Technology*: Vol. 26: Iss. 4, Article 7.
DOI: 10.6119/JMST.201808_26(4).0007
Available at: https://jmstt.ntou.edu.tw/journal/vol26/iss4/7

Journal of Marine Science and Technology, Vol. 26, No. 4, pp. 541-551 (2018)
DOI: 10.6119/JMST.201808_26(4).0007

SENSITIVITY ANALYSIS OF STEEP WAVE RISER WITH INTERNAL FLOW

Zhen Liu and Haiyan Guo

Key words: steep wave riser, buoyancy section, internal flow, effective tension.

ABSTRACT

Offshore fields, specifically, deepwater oil and gas reserves, have been receiving increasing attention with the increasing consumption of petroleum products. Marine risers are critical to the petroleum industry. The steep wave riser (SWR) is becoming increasingly popular as its use has provided a solution for oil and gas exploration in water depths where traditional rigid risers could not tolerate the environmental loads or would have become very costly. A numerical model of an SWR with internal flow is built based on the slender rod model and the finite element method. The Newton-Raphson and the Newmark-β methods are used to solve the non-linear static and dynamic problems, respectively. A calculation program, SWRNM, is developed. The results of a sensitivity analysis indicate that the buoyancy section, current, internal flow, and floater have significant effects on the SWR, and can provide guidance for future SWR designs.

I. INTRODUCTION

Global economies rely heavily on oil and gas, as oil and gas provide approximately 60% of the world energy. Offshore projects have produced approximately 30% of the oil production and 27% of the gas production since 2000; and the average water depth of these projects has increased significantly. The marine riser system is a critical component in production facilities. The steel catenary riser (SCR) is often considered as a preferable solution for riser applications in deepwater areas. Kwang and Youngseok (2017) designed an SCR system for floating production storage and offloading (FPSO) in West Africa and conducted a sensitivity analysis to improve the integrity of SCR designs. Klaycham et al. (2016) studied the nonlinear free vibration of SCRs using the finite element method. Park et al. (2015) proposed a systematic design procedure of strake configurations using the modal approach for SCRs. Bai et al. (2015) calculated the dynamic response of SCRs by numerical calculation considering stiffness degradation. Gao et al. (2011) established a simplified pinned-pinned cable vibration model to study the characteristics of SCRs. Guo and Lou (2008) studied the coupled cross-flow and in-line vortex-induced vibration of flexible pipes. However, the SCR exhibits significant tension levels at the top, and the riser is prone to fatigue damage from the severe motion of floaters and the harsh environment (Thomas et al., 2010; Felisita et al., 2017). It is challenging for an SCR to meet the criteria of both strength and fatigue in the harsh operating environment, primarily because of fatigue at the touch down zone.

The steep wave riser (SWR), lazy wave riser (LWR), steep-S riser, and lazy-S riser have all gained popularity as viable solutions to improve fatigue and strength performance of risers in deepwater areas (Bai and Bai, 2005). A wave riser configuration is generated by installing a number of buoyancy modules to a traditional SCR. The buoyancy section of the wave riser decouples the touch down point and the motion of the floater. Numerous studies have been conducted on LWRs. Torres et al. (2002) studied the application of LWRs with FPSO and they showed the LWR to have advantages in reducing fatigue damage. Li and Nguten (2010) modeled LWRs as three-segment catenary risers, however, this theory could not investigate the structural response of a riser under ocean current and internal flow. Yang and Li (2011) used the finite element method to analyze the fatigue damage of LWRs under various parameters. Sun et al. (2011) built a LWR model and conducted a parameter sensitivity analysis using OrcaFlex. Li and Li (2010) applied a three-dimensional lumped mass method to investigate the effective tension of a LWR under slow drift and dynamic platform motion, and performed a comparison between LWRs and SCRs. Santillan and Virgin (2011) modeled a steep-S and lazy-S risers using the Elastica theory and obtained the numerical results using the finite difference method. The small deformation beam theory was used to establish governing equations of LWRs, and the effect of ocean current and internal flow on the static performance of risers were studied (Wang and Duan, 2015; Wang et al., 2015). Seungjun and Moo-Hyun (2015) compared the structural performances of SCRs and LWRs under the same storm and floater conditions. However, only limited studies have been conducted on SWRs. An SWR has a steeper configuration

Paper submitted 12/19/17; revised 03/06/18; accepted 06/15/18. Author for correspondence: Haiyan Guo (e-mail: hyguo@ouc.edu.cn).
College of Engineering, Ocean University of China, Qingdao, China.

and a smaller horizontal span than a LWR and has no problem of stability in pipe-soil interactions. This type of configuration is particularly applicable to the conditions where offshore structures are densely clustered. Santillan et al. (2007) applied the finite difference method to study SWRs and modeled the buoyancy force as a concentrated force at the arch bend point. Ding et al. (2014) used OrcaFlex to perform a dynamic analysis of an SWR and analyze the effect of the buoyancy modules.

There are three primary methods for structural analysis of risers: the lumped mass method (Raman-Nair and Baddour, 2003; Yang et al., 2014), the finite difference method (Chatjigeorgiou, 2008; Santillan and Virgin, 2010), and the finite element method (Kordkheili et al., 2011; Yoo et al., 2017). The finite element method has significant advantages in handling complex configurations and boundary conditions. The slender rod model is based on the absolute coordinate system and obviates a time-consuming coordinate system transformation, that is essential in the traditional finite element method. The slender rod model was originally proposed by Nordgen (1974) and the equations were solved by the finite difference method. In 1982, Garrett reported that the finite element method can provide more accurate results. Paulling and Webster (1986) then improved this model by considering axial elongation.

The equations of motion of an SWR in a marine environment are established based on the slender rod model, with axial elongation and internal flow taken into consideration. The finite element method is used to solve the equations, and the Newton-Raphson and Newmark-β methods are used to solve the nonlinear static and dynamic problems, respectively. Based on these, a calculation process, SWR nonlinear mechanics (SWRNM), is programmed. This study considers several factors that could affect the structural response of an SWR such as buoyancy section, current, internal flow, and floater. A series of parametric studies are conducted. The primary objective of this study is to provide a technical reference for SWR design that is feasible for application in deepwater harsh environments.

II. MATHEMATICAL MODEL

1. SWR Model

A typical SWR model is presented in Fig. 1. The riser can be divided into three sections: the lower section (A-B), the buoyancy section (B-C-D), and the upper section (D-E-F). The L1 symbol in the figure depicts the length of the riser from its touch down point to the beginning of the buoyancy section, L2 the length of the buoyancy section, and L3 the length of the riser from the end of the buoyancy section to the hang-off point. The buoyancy section of the riser is subjected to greater upward buoyancy than downward gravity forces. An arch bend is generated, and the peak of the arch bend is called arch bend point. The upper section has a sag bend and the lowest point is called the sag bend point. The hang-off point of the riser is connected with a floater.

2. Slender Rod Model

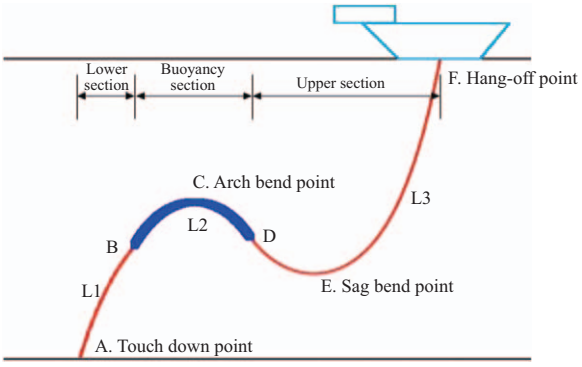

Fig. 1. Typical configuration of SWR.

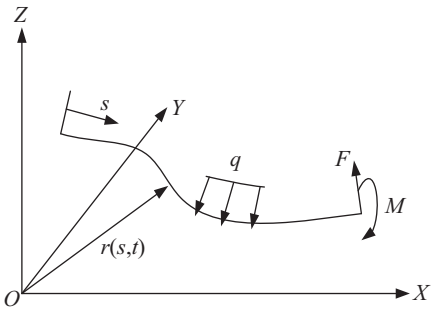

Fig. 2. Slender rod model.

The configuration of a slender rod is described in terms of the position of the center line of the rod, as shown by the space curve $\boldsymbol{r}(s, t)$ in Fig. 2. The slender rod $\boldsymbol{r}(s, t)$ is the function of the arc length s and time t. The slender rod model can accommodate great displacements effectively (Chen et al., 2011).

The internal stress state at each point along the riser is described fully by the resultant force $\boldsymbol{F}$ and the resultant bending moment $\boldsymbol{M}$, with the effects of rotary inertia and shear deformation neglected. The equations of motion of the SWR with internal flow can be derived by the conservation of linear and angular momenta. The prime and superposed dot in the equations of motion represent differentiation for arc length and time, respectively.

$$\boldsymbol{F}' + \boldsymbol{q} = (\rho + m_f)\ddot{\boldsymbol{r}} \tag{1}$$

$$\boldsymbol{M}' + \boldsymbol{r}' \times \boldsymbol{F} + \boldsymbol{m} = \boldsymbol{0} \tag{2}$$

where $\boldsymbol{q}$ is the applied force per unit length, ρ and m_f are the mass of the riser and the internal flow per unit length, respectively, and $\boldsymbol{m}$ is the applied moment per unit length.

For slender structures, torque and distributed torsional moment are usually neglected and $\boldsymbol{M} = \boldsymbol{r}' \times EI\boldsymbol{r}''$, $\boldsymbol{m} = \boldsymbol{0}$, where EI is the bending stiffness of riser, E is the elastic modulus, and I is moment of inertia.

The rod is assumed to be elastic and extensible. Therefore, the deformation condition holds:

$$\frac{1}{2}(\boldsymbol{r}'\cdot\boldsymbol{r}'\text{-}1)=\frac{T}{EA}\approx\frac{\lambda-p_oA_o+p_iA_i}{EA} \tag{3}$$

where $\lambda=T_e-EI\kappa^2$, $\kappa=\boldsymbol{r}''$ is the local curvature, $T_e=T+p_oA_o-p_iA_i$ is the local effective tension, T is the wall tension, p_o and p_i are the external and internal hydrostatic pressures, respectively, A_o and A_i are the outer and inner cross-sectional areas, respectively, EA is the axial tensile stiffness of riser, and A is the cross-sectional area.

The equation of motion of the SWR can be written as:

$$-(EI\boldsymbol{r}'')''+(\lambda\boldsymbol{r}')'+\boldsymbol{q}=(\rho+m_f)\ddot{\boldsymbol{r}} \tag{4}$$

3. Load Analysis

An SWR is subjected to various loads in the dynamic marine environment that can be divided into hydrostatic forces and hydrodynamic forces. And the riser is also subjected to gravity force. The applied force per unit length $\boldsymbol{q}$ can be expressed as follows.

$$\boldsymbol{q}=\boldsymbol{w}+\boldsymbol{F}^s+\boldsymbol{F}^d \tag{5}$$

where $\boldsymbol{w}$, $\boldsymbol{F}^s$, and $\boldsymbol{F}^d$ are the gravity, hydrostatic, and hydrodynamic forces per unit length, respectively. The buoyancy force and pressure are considered as hydrostatic forces, and the hydrodynamic forces are calculated by the Morison equation.

$$\boldsymbol{F}^s=\boldsymbol{B}+(P\boldsymbol{r}')' \tag{6}$$

$$\begin{aligned}\boldsymbol{F}^d=&\rho_w\frac{\pi D^2}{4}\dot{\boldsymbol{V}}+C_a\rho_w\frac{\pi D^2}{4}(\dot{\boldsymbol{V}}^{\boldsymbol{n}}-\ddot{\boldsymbol{r}}^{\boldsymbol{n}})\\&+\frac{1}{2}C_D\rho_wD\left|\boldsymbol{V}^{\boldsymbol{n}}-\dot{\boldsymbol{r}}^{\boldsymbol{n}}\right|(\boldsymbol{V}^{\boldsymbol{n}}-\dot{\boldsymbol{r}}^{\boldsymbol{n}})\end{aligned} \tag{7}$$

where $\boldsymbol{B}$ is the applied buoyancy force per unit length, $P=p_oA_o-p_iA_i$ is the hydrostatic pressure, that is induced by the pressure difference between outer and inner pressure, ρ_w is the density of seawater, D is the outer diameter of the riser, C_a is the added mass coefficient, C_D is the drag coefficient, $\dot{\boldsymbol{V}}$ is the acceleration of the wave and the current, $\boldsymbol{V}^{\boldsymbol{n}}$ and $\dot{\boldsymbol{V}}^{\boldsymbol{n}}$ are the normal components of the particle velocity and acceleration of the wave and the current, respectively, and $\dot{\boldsymbol{r}}^{\boldsymbol{n}}$ and $\ddot{\boldsymbol{r}}^{\boldsymbol{n}}$ are the normal velocity and acceleration of the riser with respect to its center line, respectively.

The problem of internal flow exists in both onshore and the offshore structures. The mixture of oil-gas-water with high temperatures and pressures is transported inside the riser. The effect of the internal flow is highly complex. To simplify the modeling, the internal flow is approximated as a plug flow, that is similar to an infinitely flexible rod where all points of the flow have the same velocity v. The force induced by the internal flow on the riser can be obtained according to Païdoussis (1998):

$$\boldsymbol{f}(s,t)=-m_f\frac{D^2\boldsymbol{r}}{Dt^2}=-m_f\left(\frac{\partial^2\boldsymbol{r}}{\partial t^2}+2v\frac{\partial^2\boldsymbol{r}}{\partial s\partial t}+v^2\frac{\partial^2\boldsymbol{r}}{\partial s^2}\right) \tag{8}$$

where the first term is the inertial force, the second term is associated with the Coriolis force, and the third term is associated with the centrifugal force as the flow has the same curvature as the riser.

4. Finite Element Model

The equation of motion and inextensibility condition of the SWR can be written in subscript notation as follows:

$$\begin{aligned}&-(\rho+m_f)\ddot{r}_i-C_A\dot{r}_i^n-2m_fv\dot{r}_i'-(EIr_i'')''\\&+(\lambda r_i')'+\bar{w}_i+\bar{F}_i^d=0\end{aligned} \tag{9}$$

$$\frac{1}{2}\left(r_n'r_n'-1\right)-\frac{\lambda-P+m_fv^2}{EA}=0 \tag{10}$$

The SWR is discretized into a number of elements along the arc length. The variables of a single element can be derived by:

$$r_i(s,t)=A_l(s)U_{il}(t) \tag{11}$$

$$\lambda(s,t)=P_m(s)\lambda_m(t) \tag{12}$$

where $A_l(s)$ are the Hermitian cubic shape functions, $P_m(s)$ are the Hermitian quadratic shape functions, $U_{il}(t)$ are the position and tangent vectors, and $\lambda_m(t)$ are the effective tension vectors.

The final equations for the SWR are as follows:

$$(M_{ijlk}+M_{ijlk}^a)\ddot{U}_{jk}+C_{ijlk}^f\dot{U}_{jk}+(K_{ijlk}^1+\lambda_nK_{nijlk}^2)U_{jk}-F_{il}=0 \tag{13}$$

$$A_{mil}U_{ki}U_{kl}-B_m+C_{mn}(h_n-\lambda_n)=0 \tag{14}$$

where M_{ijlk} and M_{ijlk}^a are mass matrices, K_{ijlk}^1 and K_{nijlk}^2 are stiffness matrices induced by material tension and curvature, respectively, C_{ijlk}^f is a damping matrix induced by internal flow, F_{il} is a load vector, $A_{mil}=\frac{1}{2}\int_0^L P_mA_i'A_l'ds$, $B_m=\frac{1}{2}\int_0^L P_mds$, $C_{mn}=\frac{1}{EA}\int_0^L P_mP_nds$, and $h_n=A_oP_{on}-A_iP_{in}$.

5. Static Analysis

The inertial force term is discarded in the static analysis.

$$R_{il}=(K_{ijlk}^1+\lambda_nK_{nijlk}^2)U_{jk}-F_{il}=0 \tag{15}$$

$$G_m=A_{mil}U_{ki}U_{kl}-B_m+C_{mn}(h_n-\lambda_n)=0 \tag{16}$$

Table 1. SWR properties.

Properties	Value	Properties	Value
Steel pipe density (kg/m^3)	7860	Lower section length (m)	400
Outer diameter (m)	0.20	Buoyancy section length (m)	500
Inner diameter (m)	0.18	Upper section length (m)	1500
Elastic module (GPa)	206	Seawater density (kg/m^3)	1024
Internal flow density (kg/m^3)	998	Drag coefficient	1.0
Internal flow velocity (m/s)	5	Inertia coefficient	2.0

These nonlinear algebraic equations are solved by the Newton-Raphson method, that is a classical method for solving nonlinear equations. This method assumes the unknown values in iterative step n are $U^{(n)}$ and $\lambda^{(n)}$. The values are expanded by Taylor series.

$$R_{il}^{(n+1)} = R_{il}^{(n)} + \frac{\partial R_{il}}{\partial U_{jk}}\left(\Delta U_{jk}\right) + \frac{\partial R_{il}}{\partial \lambda_n}\left(\Delta \lambda_n\right) = 0 \tag{17}$$

$$G_m^{(n+1)} = G_m^{(n)} + \frac{\partial G_m}{\partial U_{jk}}\left(\Delta U_{jk}\right) + \frac{\partial G_m}{\partial \lambda_n}\left(\Delta \lambda_n\right) = 0 \tag{18}$$

The unknown values can be obtained by loop iteration.

6. Dynamic Analysis

The equation for modal analysis without damping and load is:

$$(M_{ijlk} + M_{ijlk}^a)\ddot{U}_{jk} + (K_{ijlk}^1 + \lambda_n K_{nijlk}^2)U_{jk} = 0 \tag{19}$$

Supposing $U = \varphi e^{i\omega t}$, we have

$$(K_{ijlk}^1 + \lambda_n K_{nijlk}^2)\{\varphi\} = \omega^2 (M_{ijlk} + M_{ijlk}^a)\{\varphi\} \tag{20}$$

where ω is the natural frequency of the SWR, and $\{\varphi\}$ is the corresponding modal.

The dynamic response of the SWR is integrated in the time domain by the Newmark-β method.

(1) Initial condition
The equilibrium shape of the SWR is taken as the initial condition, and the load is applied from the zero point with the slope function.

$$u^{(0)} = 0,\ \dot{u}^{(0)} = 0,\ \ddot{u}^{(0)} = 0 \tag{21}$$

(2) Estimate.

$$\begin{aligned}
\ddot{u}^{(n)} &= \ddot{u}^{(n-1)} \\
\dot{u}^{(n)} &= \dot{u}^{(n-1)} + \Delta t(1-\gamma)\ddot{u}^{(n-1)} + \Delta t\gamma\ddot{u}^{(n)} \\
u^{(n)} &= u^{(n-1)} + \Delta t\dot{u}^{(n-1)} + \Delta t^2(0.5-\beta)\ddot{u}^{(n-1)} + \Delta t^2\beta\ddot{u}^{(n)} \\
\lambda^{(n)} &= \lambda^{(n-1)}
\end{aligned} \tag{22}$$

(3) Calculate the increment.

$$\delta^{(n)} = \left\{\delta u^{(n)}, \delta\lambda^{(n)}\right\}^T.$$

$$\delta^{(n)} = \left[K\right]^{-1}\left\{R\right\} \tag{23}$$

where $[K]$ is the stiffness matrix, and $\{R\}$ is the load vector.

(4) Correction.
The values are corrected using Eq. (24). If the incremental condition meets the convergence criteria, the next time step is calculated. Otherwise, the values have to be estimated again.

$$\begin{aligned}
u^{(n+1)} &= u^{(n)} + \delta u^{(n)} \\
\dot{u}^{(n+1)} &= \dot{u}^{(n)} + \frac{\gamma}{\beta\Delta t}\delta u^{(n)} \\
\ddot{u}^{(n+1)} &= \ddot{u}^{(n)} + \frac{1}{\beta\Delta t^2}\delta u^{(n)} \\
\lambda^{(n+1)} &= \lambda^{(n)} + \delta\lambda^{(n)}
\end{aligned} \tag{24}$$

(5) Repeat steps 2-4 until all time steps have been completed. Based on the MATLAB platform, the calculation process of the SWR is programmed into SWRNM (SWR nonlinear mechanics).

7. Model Validation

The detailed physical properties of the SWR used in this study are presented in Table 1. Both ends of the SWR are hinged.

The results calculated by OrcaFlex are used to verify the accuracy of the SWRNM. Fig. 3 shows the comparisons between SWRNM and OrcaFlex, where it can be observed that the results from the two methods are in good agreement.

III. RESULTS AND DISCUSSIONS

1. Effects of Buoyancy Section on SWR

The buoyancy section is a long length of the SWR with buoyancy modules attached. This is one of the principle factors determining the configuration of the SWR and influences the response of the SWR under marine loads. The effects of the buoyancy section on the SWR are studied in detail in this section,

Table 2. Critical results at key points with different buoyancy section diameters.

Diameter (m)	C_C (1/m)	C_E (1/m)	T_A (kN)	T_B (kN)	T_D (kN)	T_F (kN)	σ_{max} (MPa)
0.38	0.0066	0.0062	58.82	164.54	84.67	532.33	146.67
0.40	0.0073	0.0054	81.55	212.63	101.75	519.67	161.81
0.42	0.0079	0.0048	126.86	268.77	114.74	512.38	175.45

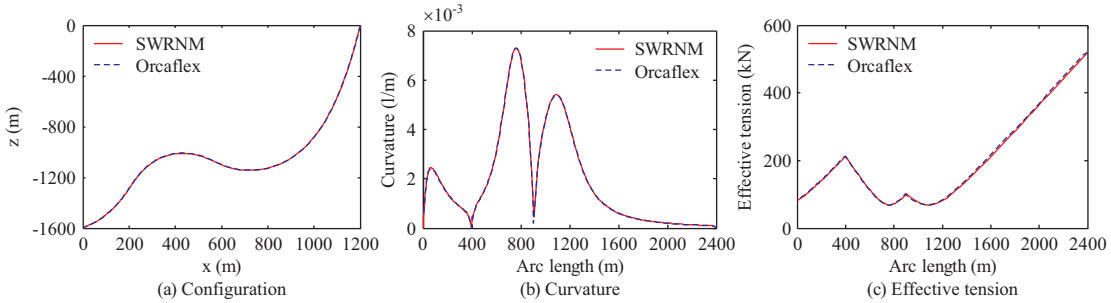

Fig. 3. Comparisons between SWRNM and OrcaFlex.

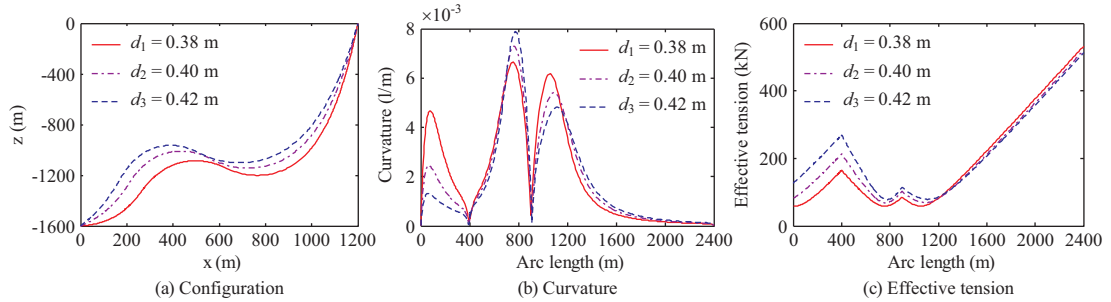

Fig. 4. Results with different buoyancy section diameters.

with buoyancy section diameter, length, and starting position considered.

1) Sensitivity to Buoyancy Section Diameter

The length of the buoyancy section is set as 500 m, and the starting position of the buoyancy section is set as 400 m away from the touch down point. Three buoyancy section diameters are tested: $d_1 = 0.38$ m, $d_2 = 0.40$ m, and $d_3 = 0.42$ m. The configuration, curvature, and effective tension of the SWR are calculated for the three diameters.

Fig. 4 shows the configuration, curvature, and effective tension of the SWR along the arc length. Table 2 presents the curvature of the SWR at the arch bend point (point C) and the sag bend point (point E). With increasing buoyancy section diameter, the buoyancy provided by the buoyancy section increases, that leads to the SWR buoyancy section rising. The curvature at the arch bend point increases, while the curvature at the sag bend point decreases. Table 2 also shows the effective tension at the touch down point (point A), the buoyancy section starting point (point B), the buoyancy section ending point (point D), and the hang-off point (point E). The results indicate that the tension at the hang-off point decreases with increasing buoyancy section diameter, reducing the effective tension at the hang-off point. However, the effective tension of the lower and buoyancy sections increases with increasing buoyancy section diameter. The results in Table 2 also indicate that the effect of the buoyancy section diameter on the effective tension at the touch down point is greater than the effective tension at the hang-off point. It can be seen that the effective tension of the lower and the buoyancy sections is more sensitive to the change of the buoyancy section diameter than the effective tension of the upper section. The maximum stress σ_{max} along the riser increases with increasing buoyancy section diameter.

2) Sensitivity to Buoyancy Section Length

Different SWR buoyancy section lengths are investigated in this section. The buoyancy section lengths used in the numerical simulation are $l_1 = 400$ m, $l_2 = 500$ m, and $l_3 = 600$ m. The configuration, curvature, and effective tension of the SWR with the different lengths are shown in Fig. 5.

As the buoyancy section length increases, the SWR rises significantly and the buoyancy section becomes straighter. Table 3 shows that the curvature at the arch bend and sag bend points decreases with increasing buoyancy section length. The

Table 3. Critical results at key points with different buoyancy section lengths.

Length (m)	C_C (1/m)	C_E (1/m)	T_A (kN)	T_B (kN)	T_D (kN)	T_F (kN)	σ_{max} (MPa)
400	0.0076	0.0057	64.72	166.71	93.28	565.86	168.04
500	0.0073	0.0054	81.55	212.63	101.75	519.67	161.81
600	0.0070	0.0051	121.21	264.39	106.35	479.03	155.54

Table 4. Critical results at key points with different buoyancy section starting positions.

Starting position (m)	C_C (1/m)	C_E (1/m)	T_A (kN)	T_B (kN)	T_D (kN)	T_F (kN)	σ_{max} (MPa)
300	0.0067	0.0050	111.69	213.83	107.69	558.31	151.34
400	0.0073	0.0054	81.55	212.63	101.75	519.67	161.81
500	0.0080	0.0060	61.80	213.92	93.94	483.42	174.54

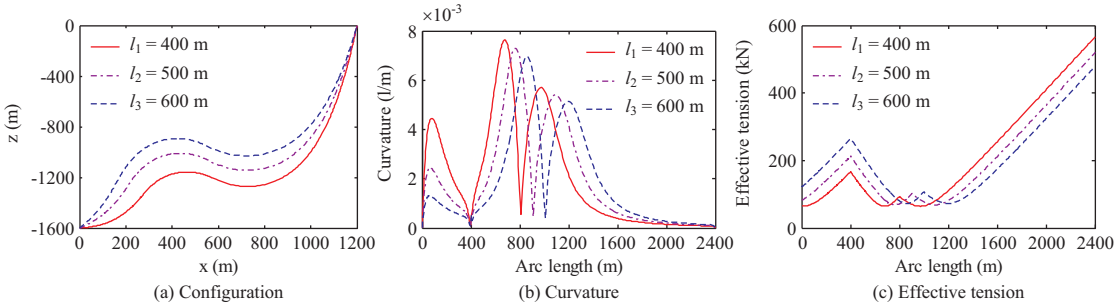

Fig. 5. Results with different buoyancy section lengths.

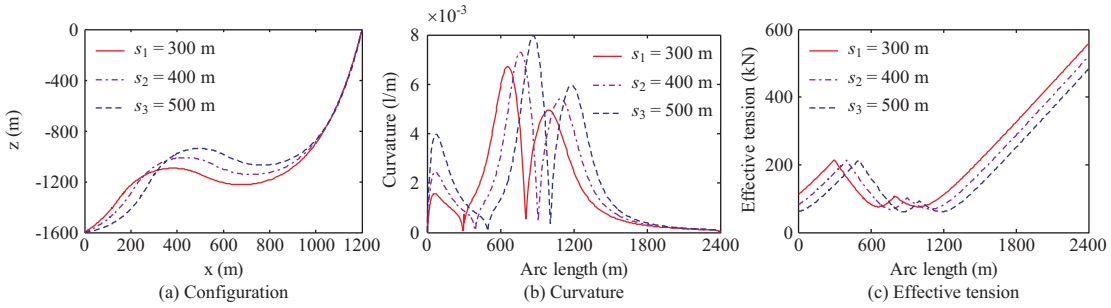

Fig. 6. Results with different buoyancy section starting positions.

SWR effective tension at key points (A, B, D, and F) with different buoyancy section lengths is also presented in Table 3. The effective tension is sensitive to the changes in the buoyancy section length. With increasing buoyancy section length, the effective tension at the touch down point increases, while the effective tension at the hang-off point has an apparent decrease. However, the maximum stress along the riser also decreases. This indicates that longer buoyancy section can reduce the maximum tension requirements and the maximum stress of the riser.

3) Sensitivity to Buoyancy Section Starting Position

Based on the same diameter and length of a buoyancy section, three different buoyancy section starting positions are considered. Three distances between the touch down point and buoyancy section starting position (the length from point A to point B) are selected: s_1 = 300 m, s_2 = 400 m, and s_3 = 500 m.

Fig. 6 shows the change configuration, curvature and effective tension of the SWR for different buoyancy section starting positions. It can be seen from Fig. 6 and Table 4 that when the length between touch down point and buoyancy section starting position increases, the SWR rises and the curvature at the arch bend and sag bend points increases, and the effective tension at the touch down and hang-off points decreases. The maximum stress along the riser increases with increasing length as shown in Table 4. As a result, the location of the buoyancy section requires careful consideration.

2. Effects of Ocean Current on SWR

Ocean current could cause a riser to offset because of drag and other hydrodynamic forces. In this analysis, three ocean cur-

Table 5. Critical results at key points with different current velocities.

Current velocity (m/s)	C_C (1/m)	C_E (1/m)	T_A (kN)	T_B (kN)	T_D (kN)	T_F (kN)	σ_{max} (MPa)
0	0.0073	0.0054	81.55	212.63	101.75	519.67	161.81
0.4	0.0072	0.0054	89.01	214.01	101.11	523.63	159.42
0.8	0.0066	0.0050	111.35	219.33	101.02	536.68	149.10

Table 6. Results with different internal flow velocities.

Velocity (m/s)	ω_1 (rad/s)	ω_2 (rad/s)	ω_3 (rad/s)	C_C (1000/m)	C_E (1000/m)	T_A (kN)	T_F (kN)
0	0.0490	0.0890	0.1317	7.29562	5.41486	81.5538	519.6738
10	0.0486	0.0881	0.1301	7.29568	5.41491	81.5530	519.6731
20	0.0471	0.0853	0.1251	7.29585	5.41505	81.5507	519.6712
30	0.0445	0.0802	0.1160	7.29615	5.41528	81.5469	519.6679

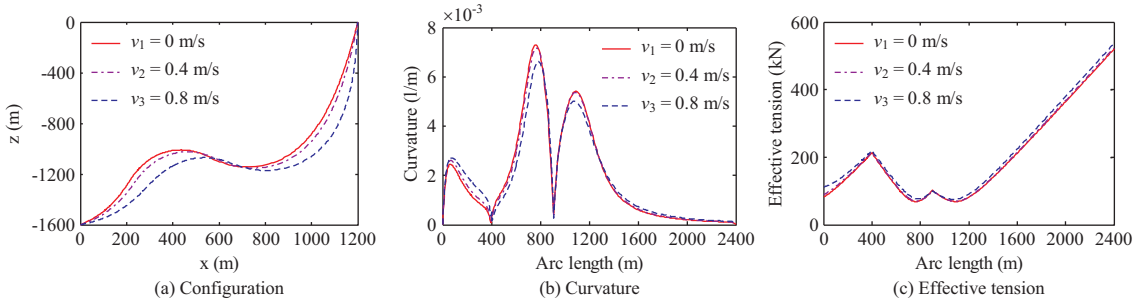

Fig. 7. Results with different current velocities.

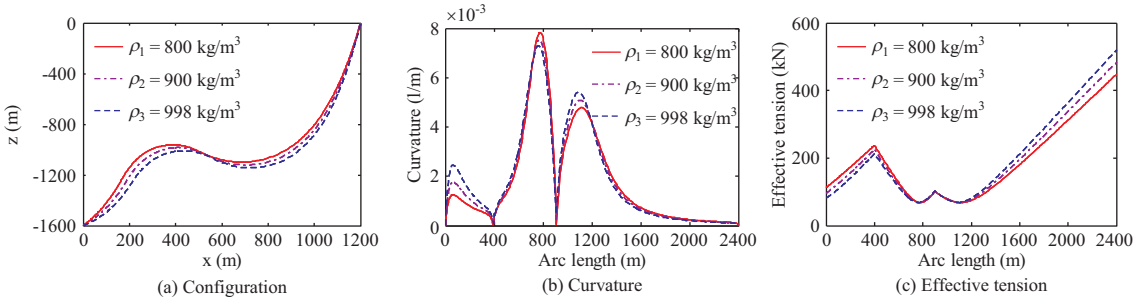

Fig. 8. Results with different internal flow densities.

rent velocities are applied to the SWR to study the effect of ocean current: $v_1 = 0$ m/s, $v_2 = 0.4$ m/s, and $v_3 = 0.8$ m/s. Table 5 presents the critical results of the SWR at key points with different current velocities. The configuration, curvature, and effective tension of the SWR are studied and the results are shown in Fig. 7.

As can be seen from Fig. 7, the ocean current has a significant effect on the configuration of an SWR, however, it has a minimal effect on the effective tension of an SWR. As the current velocity increases along the +x direction, the shape of the SWR becomes straighter, the curvature at arch bend and sag bend points decreases, and the effective tension increases marginally along the riser. The maximum stress along the riser decreases with increasing current velocity. As a result, ocean current velocity should be taken into consideration during the design stage.

3. Effect of Internal Flow on SWR

1) Sensitivity to Internal Flow Velocity

The effect of internal flow on the SWR is considered. Four different internal flow velocities ranging from 0-30 m/s were selected for analysis. The first order to third order natural frequencies, curvatures at the arch bend and sag bend points, effective tensions at the touch down and hang-off points of the SWR for the different internal flow velocities are presented in Table 6.

It can be seen from Table 6 that the natural frequency of the SWR decreases with increasing internal flow velocity. This is a result of the increasing internal flow velocity causing an effective tension decrease, resulting in a decrease in stiffness and a reduction in the natural frequency of the SWR. Although the internal flow velocity of the riser can never be too significant,

Table 7. Critical results at key points with different internal flow densities.

Density (kg/m^3)	C_C (1/m)	C_E (1/m)	T_A (kN)	T_B (kN)	T_D (kN)	T_F (kN)	σ_{max} (MPa)
800	0.0078	0.0048	112.96	237.40	100.78	447.68	173.04
900	0.0075	0.0051	95.48	224.45	101.79	483.55	167.09
998	0.0073	0.0054	81.55	212.63	101.75	519.67	161.81

Table 8. Critical results at key points with different floater positions.

Floater position	C_C (1/m)	C_E (1/m)	T_A (kN)	T_B (kN)	T_D (kN)	T_F (kN)	σ_{max} (MPa)
Near	0.0083	0.0062	70.88	205.83	98.21	514.57	180.33
Mean	0.0073	0.0054	81.55	212.63	101.75	519.67	161.81
Far	0.0064	0.0047	94.72	221.68	107.04	526.50	144.50

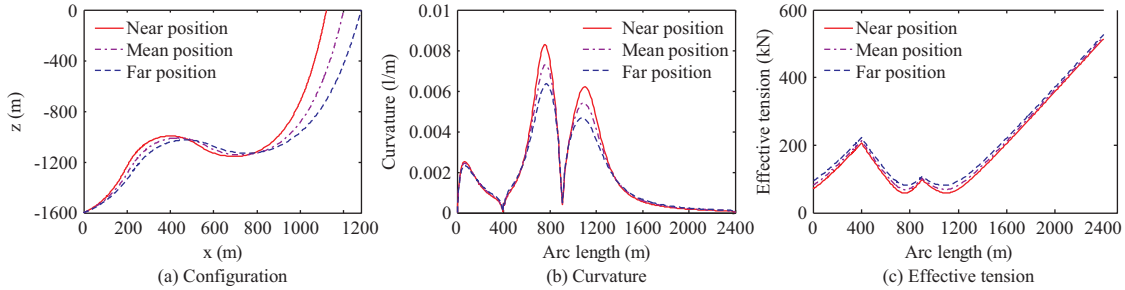

Fig. 9. Results with different floater positions.

the natural frequency of the riser may be reduced to the "lock" frequency range, generating power amplification. The internal flow velocity has little effect on the curvature and effective tension of the SWR, as the internal flow velocity is limited to a certain range.

2) Sensitivity to Internal Flow Density

Internal flow densities of ρ_1 = 800 kg/m^3, ρ_2 = 900 kg/m^3, and ρ_3 = 998 kg/m^3 are analyzed in this section. The calculated results are as shown in Fig. 8 and Table 7.

It can be seen in Fig. 8 that the SWR drops with increasing internal flow density. Compared to the internal flow velocity, the internal flow density has a greater effect on the SWR. The effective tension at the touch down point and the maximum stress along the riser decrease with increasing internal flow density, while the effective tension at the hang-off point increases significantly. Therefore, the effect of internal flow density on the SWR should be considered during the design phase.

4. Effect of Floater Offset and Motion on SWR

For the SWR, the floater offset is a static load while the floater motion is a dynamic load. The static offset is an average drift of the floater from wind, wave, and current. The floater motion includes wave frequency motion, low frequency motion, and heave motion caused by the combined effects of the first-order wave force, wind, and the second-order wave force, because of mooring line and floater offset.

The tension leg platform, as an example, has a low lateral stiffness but a high vertical stiffness, that is semi-rigid and semi-compliant, and has a significant offset in the marine environment. If the floater is regarded as a rigid body, the floater motion can be divided primarily into surge, sway, heave, roll, pitch, and yaw. In this section the effects of floater offset and floater motion, such as surge and sway, are studied.

1) Sensitivity to Floater Offset

It is assumed that the near and far positions are both 80 m (5% of the depth) from the mean position of the platform. The configuration, curvature, and effective tension of the SWR are studied when the floater is in the near position, the mean position, and the far position (See Fig. 9).

As the floater drifts from the near position to the far position, the horizontal span of the SWR increases and riser becomes straighter. According to Table 8, the curvature at the arch bend and sag bend points, and the maximum stress along the riser decrease, while the effective tension along the arc length increases marginally. This implies that the maximum strain of the SWR can be determined by the maximum tension in the far position, and the minimum bending radius can be determined by the maximum bending curvature in the near position.

2) Sensitivity to Floater Motion

In a harsh marine environment, floater motion under the combined effects of wave, current, and wind is a significant challenge for an SWR. Floater motion can be recognized as a dynamic boundary condition of a riser when investigating the dynamic

Table 9. Effective tension under floater motion.

Motion	Period (s)	Effective Tension (kN)	Compared with static response
Surge	64	483.31-552.18	8.11%
Sway	64	488.50-544.15	6.54%
Surge	128	510.77-526.41	1.30%
Sway	128	514.06-522.11	0.47%

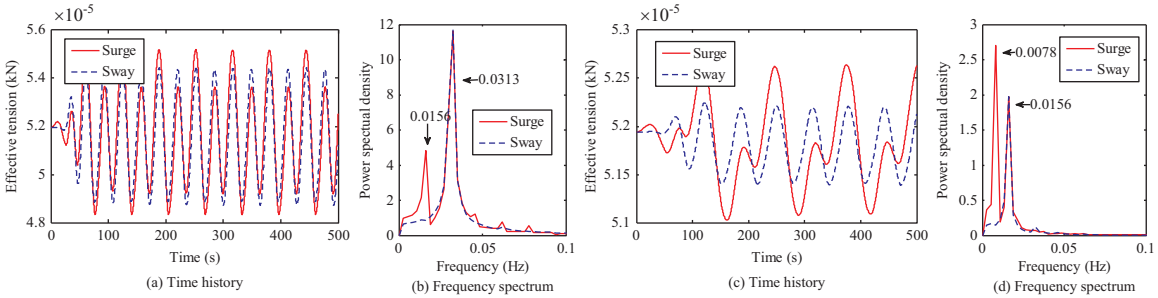

Fig. 10. Effective tension at hang-off point under floater motion: (a)-(b) T = 64 s, (c)-(d) T = 128 s.

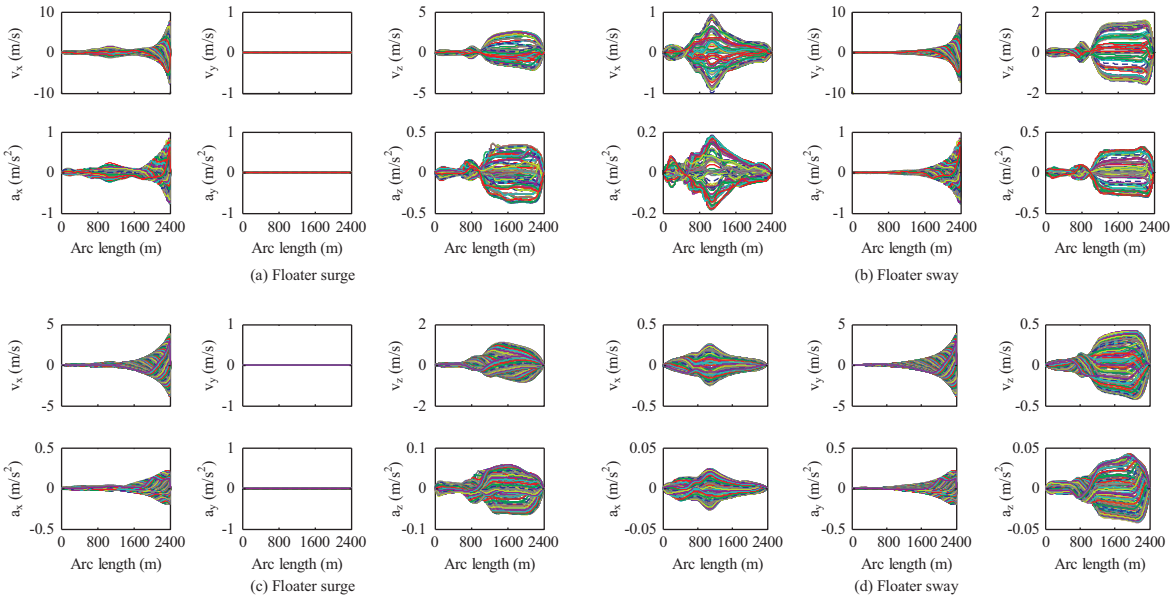

Fig. 11. Velocity and acceleration of SWR under floater motion: (a)-(b) T = 64 s, (c)-(d) T = 128 s.

response of an SWR under floater motion. The hang-off point of the SWR is subjected to a simple harmonic motion with amplitude 80 m, and periods 64 s and 128 s. Fig. 10 shows the maximum effective tension under floater surge and sway. Fig. 11 shows the velocity and acceleration in three directions.

As can be seen from Fig. 10, the effective tension of the SWR oscillates at the first period. This is a result of loads being applied by the ramp function from zero in order to eliminate the influence of a transient response. After a period, the loads attain a constant value. The effective tension of the SWR changes periodically because of the cyclic loads. The variation period of the effective tension is the same as the period of the floater surge, while the variation period of the effective tension is the half period of the floater sway as the SWR is symmetrical in the xz-plane, as seen in Fig. 2. The amplitude of the effective tension under floater surge is greater than the amplitude of the effective tension under floater sway.

The effective tension at the hang-off point is the maximum tension along the riser. Table 9 presents the values of the effective tension at the hang-off point under floater motion. As can be seen from the table, when the motion period is 64 s, the effective tension of SWR under floater surge and sway ranges from 483.31-552.18 kN and 488.50-544.15 kN, respectively, that are 8.11% and 6.54% greater than the effective tension of

Table 10. Maximum curvature, effective tension, and stress with different buoyancy sections.

	Diameter (m)			Length (m)			Starting position (m)		
	0.38	0.40	0.42	400	500	600	300	400	500
C_{Max} (1/m)	0.0066	0.0073	0.0079	0.0076	0.0073	0.0070	0.0067	0.0073	0.0080
T_{Max} (kN)	532.33	519.67	512.38	565.86	519.67	479.03	558.31	519.67	483.42
σ_{max} (MPa)	146.67	161.81	175.45	168.04	161.81	155.54	151.34	161.81	174.54

the static response, respectively. When the motion period is 128 s, the effective tension of the SWR under floater surge and sway ranges from 510.77-526.41 kN and 514.06-522.11 kN, that are 1.30% and 0.47% greater than the effective tension of the static response, respectively. As the motion period increases, the amplitude of the effective tension decreases, and the effective tension tends to 519.67 kN, that is the effective tension at the hang-off point of the static response. In a harsh marine environment, the significant motion of the floater should be carefully considered in the design phase.

As can be seen from Fig. 11, the acceleration dynamic distribution is highly similar to the velocity dynamic distribution. The velocity and acceleration of the upper section are significantly greater than the velocity and acceleration of the buoyancy section and the lower section. The velocity and acceleration exhibit sudden decreases behind the buoyancy section, specifically when the riser under the floater surges. It can be shown, once again, that the wave riser could effectively reduce the effects of the floater motion on the touch down point. This is one of the advantages of the wave riser. As the SWR is located in the xz-plane, floater surges excite the velocity and acceleration of the riser in the x- and z-directions, and floater sway excites the velocity and acceleration of the riser in the x-, y-, and z-directions. The smaller the floater motion period, the greater the velocity and acceleration of the riser. When the period changes from 128 s to 64 s, the velocity and acceleration more than double.

IV. CONCLUSIONS

In this study, the equations of motion for an SWR in a marine environment are established based on the slender rod model and solved by a finite element method. Based on these, a calculation process, SWRNM, is programmed. The study explores the effects of buoyancy section, current, internal flow, and floater on an SWR. The peak values of curvature, effective tension, and stress are the primary critical factors for the design of an SWR. In this analysis, the maximum curvature of an SWR along the arc length occurs at the arch bend point, and the maximum effective tension occurs at the hang-off point. The critical results are summarized below.

(1) Effect of floater section
Table 10 shows the maximum curvature, effective tension, and stress of an SWR with different floater sections. The buoyancy section diameter, length, and starting position directly affect the buoyancy force that the SWR is subjected to, changing the configuration, curvature, effective tension, and stress of the riser. As can be seen from Table 10, increasing diameter, length, and starting position decrease the maximum effective tension. The results differ for maximum curvature and stress. Increasing diameter and starting position cause an increase in the maximum curvature and stress, while increasing length causes a decrease in these two factors. Based on the above analysis, a designer of an SWR should choose a suitable buoyancy section diameter, length, and starting position in order to provide a suitable buoyancy force.

(2) Effect of current velocity
As the current velocity increases from 0-0.8 m/s in the +x direction, the maximum curvature decreases from 0.0073 m^{-1} to 0.0066 m^{-1}, the maximum effective tension increases from 519.67 kN to 536.68 kN, and the maximum stress decreases from 161.81 MPa to 149.10 MPa. When designing the riser, the current should be considered according to the SWR location.

(3) Effect of internal flow
The natural frequency of an SWR decreases with increasing internal flow velocity. As the actual internal flow velocity cannot be too great, the curvature and effective tension exhibit only marginal changes. When the internal flow density increases from 800 kg/m^3 to 998 kg/m^3, the SWR droppes, the effective tension at the hang-off point increases significantly from 447.68 kN to 519.67 kN, and the maximum stress along the riser decreases from 173.04 MPa to 161.81 MPa. The internal flow density has a greater effect on the SWR than the internal flow velocity.

(4) Effect of floater offset and motion
When the floater drifts from the near position to the far position, the maximum curvature decreases from 0.0083 m^{-1} to 0.0064 m^{-1}, the maximum effective tension increases from 514.57 kN to 526.50 kN, and the minimum effective tension decreases from 180.33 MPa to 144.50 MPa. As a result, the maximum strain of an SWR is determined by the maximum tension in the far position, and the minimum bending radius of an SWR is determined by the maximum bending curvature in the near position.

The maximum effective tension of an SWR under floater surge and sway changes periodically. The velocity and acceleration of the upper section are significantly greater than the velocity and acceleration of the buoyancy and lower sections. The shorter the floater motion period, the greater the velocity and acceleration of the riser, and the greater the effective tension.

Overall, the buoyancy section of an SWR should receive significant consideration during the design stage. In the marine environment, an SWR is subjected to significant challenges from ocean current, internal flow, and floater. These factors must be addressed in the design phase.

ACKNOWLEDGEMENTS

This study was supported by the National Natural Science Foundation of China (Grant No. 51279187), the Science and Technology Major Project of Shandong Province (Grant No. 2015ZDZX04003), and the Key Research and Development Program of Shandong Province (Grant No. 2018GHY115045).

REFERENCES

Bai, X. L., W. P. Huang, M. A. Vaz, C. Yang and M. L. Duan, (2015). Riser-soil interaction model effects on the dynamic behavior of a steel catenary riser. Marine Structures, 53-76.

Bai, Y. and Q. Bai, (2005). Subsea pipelines and risers, ELSEVIER Ltd.

Chatjigeorgiou, I. K. (2008). A finite differences formulation for the linear and nonlinear dynamics of 2D catenary risers. Ocean Engineering 35, 616-636.

Chen, H. F., S. P. Xu and H. Y. Guo (2011). Nonlinear analysis of flexible and steel catenary risers with internal flow and seabed interaction effects. Journal of Marine Science and Application, 34-40.

Ding, P. L., Y. Li and Z. L. Liu (2014). Optimization for buoyancy modulus of dynamic flexible risers with steep-wave configuration and its application. The Ocean Engineering, 1-4. (in Chinese)

Felisita, A., O. T. Gudmestad, D. Karunakaran and L. O. Martinsen (2017). Review of steel lazy wave riser concepts for North Sea. ASME 2015 International Conference on Ocean, Offshore and Arctic Engineering.

Gao, Y., Z. Zong and L. Sun (2011). Numerical prediction of fatigue damage in steel catenary riser due to vortex-induced vibration. Journal of Hydrodynamics Ser. B, 154-163.

Garrett, D. L. (1982). Dynamic analysis of slender rods. Journal of Energy Resources Technology 104, 302-306.

Guo, H. Y. and M. Lou (2008). Experimental study on coupled cross-flow and in-line vortex-induced vibration of flexible risers. China Ocean Engineering, 123-129.

Kim, S. and M. H. Kim (2015). Dynamic behaviors of conventional SCR and lazy-wave SCR for FPSOs in deepwater. Ocean Engineering, 396-414.

Klaycham, K., C. Athisakul and S. Chucheepsakul (2016). Nonlinear vibration of marine riser with large displacement. Journal of Marine Science and Technology, 1-15.

Kordkheili, S. A. H., H. Bahai and M. Mirtaheri (2011). An updated Lagrangian finite element formulation for large displacement dynamic analysis of three-dimensional flexible riser structures. Ocean Engineering 38(5-6), 793-803.

Kwang, K. Y. and J. Youngseok (2017). Sensitivity study on SCR design for spread-moored FPSO in West Africa. Journal of Ocean Engineering and Technology, 111-120.

Li, S. C. and C. Nguten (2010). Dynamic response of deepwater lazy-wave catenary riser. DOT-Deep Offshore Technology International Conference.

Li, Y. and X. Li (2014) Nonlinear analysis of lazy-wave steel catenary riser in seepwater. Shipbuilding of China, 92-101. (in Chinese)

Nordgren, R. P. (1974). On Computation of the motion of elastic rods. Journal of Applied Mechanics 41(3), 777-780.

Païdoussis, M. P. (1998). Fluid-structure interactions, Volume 1. slender structures and axial flow. California Academic Press, Millbrae.

Park, K. S., Y. T. Kim, D. K. Kim, S. Y. Yu and H. S. Choi, (2015). A new method for strake configuration design of Steel Catenary Risers. Ships & Offshore Structures, 385-404.

Paulling, J. R. and W. C. Webster (1986). A consistent large amplitude analysis of the coupled response of a TLP and Tendon System. Proceedings of the 5th OMAE Symposium, Japan, vol. III, 126-133.

Raman-Nair, W. and R. E. Baddour (2003). Three-dimensional dynamics of a flexible marine riser undergoing large elastic deformations. Multibody System Dynamics 10 (3), 393-423.

Santillan, S. T., L. N. Virgin and R. H. Plaut (2007). Static and dynamic behavior of highly deformed risers and pipelines. ASME 2007 26th International Conference on Offshore Mechanics and Arctic Engineering, American Society of Mechanical Engineers, 143-149.

Santillan, S. T. and L. N. Virgin (2011). Numerical and experimental analysis of the static behavior of highly deformed risers. Ocean Engineering 38(13), 1397-1402.

Sun, L. P., J. Zhou and J. Q. Wang (2011). Lazy wave configuration and parameter sensitivitiy analysis of deepwater flexible riser. China Offshore Platform, 37-42. (in Chinese)

Thomas, B., A. Benirschke and T. Sarkar (2010). Parque das Conchas (BC10) Steel Lazy Wave Riser Installation: Pre-Abandonment, Recovery and Transfer Challenges. Offshore Technology Conference.

Torres, A. L. F. L., E. C. Gonzalez, M. Q. D. Siqueira, C. M. S. Dantas, M. M. Mourelle and R. M. C. D. Silva (2002). Lazy-wave steel rigid risers for turret-moored FPSO. ASME 2002 International Conference on Offshore Mechanics and Arctic Engineering.

Wang, J. L. and M. L. Duan (2015). A nonlinear model for deepwater steel lazy-wave riser configuration with ocean current and internal flow. Ocean Engineering, 155-162.

Wang, J. L., M. L. Duan and J. M. Luo (2015). Mathematical model of steel lazy-wave riser abandonment and recovery in deepwater. Marine Structures, 127-153.

Yang, C., Y. X. Wang and W. G. Zuo (2014). Numerical simulations on the motion of immerged tunnel element with different arrangement types of mooring lines. The Ocean Engineering 32(1), 32-40. (in Chinese)

Yang, H. Z. and H. J. Li (2011). Sensitivity analysis of fatigue life prediction for deepwater steel lazy wave catenary risers. Technological Sciences, 1881-1887.

Yoo, D. H, B. S. Jang and K. H. Yim (2017). Nonlinear finite element analysis of failure modes and ultimate strength of flexible pipes. Marine Structures 54, 50-72.